High-temperature oxidation and quenching of chromium-coated zirconium alloy ATF cladding tubes with and w/o pre-damage

M. Steinbrück [a,*], U. Stegmaier [a], M. Große [a], L. Czerniak [b], E. Lahoda [b], R. Daum [c], K. Yueh [c]

[a] *Karlsruhe Institute of Technology, Germany*
[b] *Westinghouse Electric Company, USA*
[c] *Electric Power Research Institute, USA*

A B S T R A C T

Chromium-coated zirconium alloys are one of the promising candidates for accident-tolerant fuel cladding (ATF) tubes for light water reactors (LWRs). In this study, the high temperature oxidation and degradation of two types of Cr coatings (cold spray and physical vapor deposition) with and without pre-damage by scratches were investigated on prototype rod segment samples filled with ZrO_2 pellets and tightly sealed with welded end caps. Isothermal tests at 1100 and 1200 °C were terminated by quenching with water; transient tests were performed up to 1500–1600 °C until complete coating failure. The positive effect of both types of Cr coatings was observed in all tests. Pre-damaged specimens showed only locally increased oxidation of the scratched zone, but no negative effects on the adjacent Cr coating. The behavior of the two types of coatings is compared and the degradation mechanisms are discussed based on hydrogen release data, extensive metallographic post-test examinations, and the current state of global research.

1. Introduction

Chromium (Cr) coated zirconium alloys (Zry) are one of the promising candidates for application as accident-tolerant fuel (ATF) cladding in LWRs. They offer a near-term, rather evolutionary solution with the highest Technology Readiness Level (TRL) among the concepts worldwide discussed for ATF cladding [1–3]. There is a large number of publications showing the positive effect of chromium coating on the high-temperature oxidation resistance of zirconium alloy cladding tubes and discussing the corresponding mechanisms, e.g. [4–14]. More citations are given in the State-of-the Art-Reports by OECD-NEA [15] and PNNL [16]. The oxidation kinetics of Cr coated materials is reduced by 1,2 orders of magnitude compared to uncoated Zr alloys up to temperatures of 1200 °C. The protective effect of the Cr layer relies on the formation of a Cr_2O_3 superficial layer. It is maintained as long as the layer is not consumed by oxidation, interaction with the Zry substrate and, at very high temperatures, potentially by volatilization. Generally, Cr-coatings obtained by application of different methods effectively act as diffusion barrier against oxygen ingress, although it has to be mentioned that the protective effect of the coating is strongly dependent on the selection of appropriate deposition process parameters and the thickness of the coating [4,9].

The degradation of Cr coatings as well as the limits of the protective effect of Cr coatings at very high temperatures are determined by the Zr-Cr phase diagram [17]. First, the lowest eutectic temperature in the system is at about 1330 °C. This seems to be the ultimate maximum temperature for the protective effect of chromium coating, because beyond this temperature liquid phase is formed. Second, the intermetallic phase $ZrCr_2$ is formed in three allotropic forms. Intermetallics are known to form high hardness, brittleness, and strength that could affect the behavior of the cladding during high-temperature scenarios. Third, the solubility of Zr in chromium is low, but the solubility of Cr in zirconium in the β-Zr temperature range is considerable reaching 8.4 at.% (4.6 wt.%) at the eutectic temperature. Both, the formation of the intermetallic compound as well as the diffusion of Cr into the zirconium bulk lead to the consumption of the chromium coating by relocation to the inner side at high temperatures. These effects have been separately investigated recently by Yang et al. [18].

Brachet et al. [19] investigated the oxidation behavior of chromium-coated M5® alloy during steam oxidation at temperatures above 1300 °C. The main outcome was that the zirconia formation below the wavy Cr layer is very homogeneous and the oxidation kinetics after failure of the coating is approximately the same as the oxidation kinetics of uncoated zirconium alloys at the same conditions. A “crocodile skin” surface of such samples after oxidation at >1300 °C has been observed.

* Corresponding author.
E-mail address: martin.steinbrueck@kit.edu (M. Steinbrück).

Table 1
Test matrix and selected results.

Sample	Time & temp.	Nominal Cr thickness, µm	Termi-nation	Mass change, g	H_2, ml	Remarks
uncoated	transient up to 1532 °C	0	HF off	2.0021	2300 *(1845*)*	
CS	transient up to 1525 °C	25	HF off	-	1475 *(1421*)*	Sample broke during unscrewing
CS-D	transient up to 1554 °C	25	HF off	1.4307**	1737 *(1299*)*	Sample broke during unscrewing
PVD	transient up to 1579 °C	10	HF off	1.6375**	1949 *(1270*)*	Sample broke during handling
uncoated	1 h @1100 °C	0	quench	0.3422	509.4	HF turned off a few seconds later than planned
CS	1 h @1100 °C	25	quench	-0.0153	46.7	Probably post-test loss of small sample part
PVD	1 h @1100 °C	10	quench	0.0382	47.4	H_2 release started during heating because of residual humidity in the test section
PVD-D	1 h @1100 °C	10	HF off	0.0030	64.1	
Uncoated	1 h @1200 °C	0	quench	0.6280**	947.8	Sample broke during disassembling
CS	1 h @1200 °C	25	quench	0.0676	84.5	
CS-D	1 h @1200 °C	25	quench	0.0750	83.9	
PVD	1 h @1200 °C	10	quench	0.1910	205.6	Oxide scale spalled off during unscrewing
PVD-D	1 h @1200 °C	10	quench	0.2113	220.3	

HF off means high frequency power switched off
* at 1525 °C.
** Mass change including Zry-4 capillary.

Another potential degradation mechanism of the chromium coating is the volatilization of the formed chromia layer at high temperatures resulting in paralinear oxidation kinetics [20]. Volatilization of chrome trioxide, CrO_3, in dry oxidizing conditions, and of chrome oxyhydroxides, e.g. $CrO_2(OH)_2$, in steam-rich atmospheres may cause formation of thinner oxide scales and higher metal recession, than expected from the parabolic growth kinetics [21,22]. Even Brachet et al. [5] stated, that chromium volatilization during oxidation in steam could be neglected for temperatures at least up to 1300°C, it may play a role at higher temperatures.

Most investigations on high temperature oxidation and degradation so far have been conducted isothermally with small samples. This study presents the results of isothermal tests at 1100 and 1200 °C as well as transient tests up to 1600 °C with 10 cm long Cr-coated cladding tube segments allowing only prototypic external oxidation. The isothermal tests were finished by quenching with water; the transient tests were terminated after massive failure of the cladding. Two types of Cr coatings were investigated, which were prepared by cold spraying (CS) and by physical vapor deposition (PVD) with different thicknesses. Furthermore, the effect of pre-damage of the coatings by scratches was analyzed.

2. Experimental details

2.1. Samples

Thirteen sample tubes (approximately 10 cm long) were provided by Westinghouse Electric Company LLC (WEC). They included uncoated Optimized ZIRLO™ and Cr-coated Optimized ZIRLO produced by cold spray and PVD, Table 1. The nominal thickness of the cold-sprayed Cr coatings was 25 µm and that of the PVD coatings 10 µm. The CS samples were polished, as it is part of the manufacturing process. The interface roughness for the cold spray process required a thicker coating to ensure a minimum Cr coating thickness of 10 µm. Four samples were pre-damaged with scratches (intentionally going through the coating) in the middle part of the tube samples using a Dremel. All samples were filled with zirconia pellets, simulating fuel pellets and welded leak-tight with end plugs. Welding was performed on uncoated zirconium end plugs and uncoated sections of the tube by laser welding. The welds behaved inconspicuously in all tests, but were not the subject of detailed examinations. Fig. 1 shows macro-images of all sample types investigated with smooth surfaces of the coated samples except at the pre-damaged regions.

A thread was cut in the upper plug for the connection to a capillary made of Zircaloy-4 with which the samples were suspended in the facility. By this procedure, a small hole was produced through the plug allowing pressure compensation during the HT experiments and avoiding ballooning and collapsing of the samples at high temperatures. Hence, the inner pressure inside the cladding tubes was always the same as the pressure in the quartz glass tube, i.e. slightly above normal pressure. After testing, no internal oxidation was observed across this small orifice. A thermocouple (TC) of type B (Pt30%Rh/Pt6%Rh) was fixed to the surface of each sample by a Pt30%Rh wire, Fig. 2a.

2.2. Experimental facility and test conduct

The tests were conducted in the QUENCH-SR (single rod) facility at KIT [23] with inductive heating and the possibility of quenching of the sample by a rising water cylinder, see schematic design in Fig. 2b. The sample is enclosed in a quartz glass tube allowing observation of the test by video recording. A water-cooled copper coil surrounding the glass tube generates a magnetic field inducing eddy currents in the metallic sample. Power is provided by a high frequency (HF) generator with a power of 20 kW working at a frequency up to 700 kHz. Temperature is measured and controlled via a two-color pyrometer and additionally measured by a surface TC as described above and further discussed below. The pyrometer applied is a two-color device (type IGAR 12-LO MB22), which works without knowing the emissivity of the sample surface and automatically corrects changing conditions e.g. by steam atmosphere or contaminated quartz glass. It has a measuring range of 500 to 2200 °C and works at the wavelengths 1.28 and 1.65 µm.

Some words have to be said about the temperature measurements. As already mentioned, temperature was measured (1) by one type B thermocouple attached to the surface of the sample in the middle (hottest) position and (2) by a two-color pyrometer with the spot on almost the same sample elevation but on the opposite side of the tube. Temperature control and measurement in the QUENCH-SR is less accurate compared to e.g. a homogeneously heated tube furnace. Direct inductive heating of samples is dependent on the properties of the samples, especially the electrical resistance and the homogeneity of the sample. Pretests were

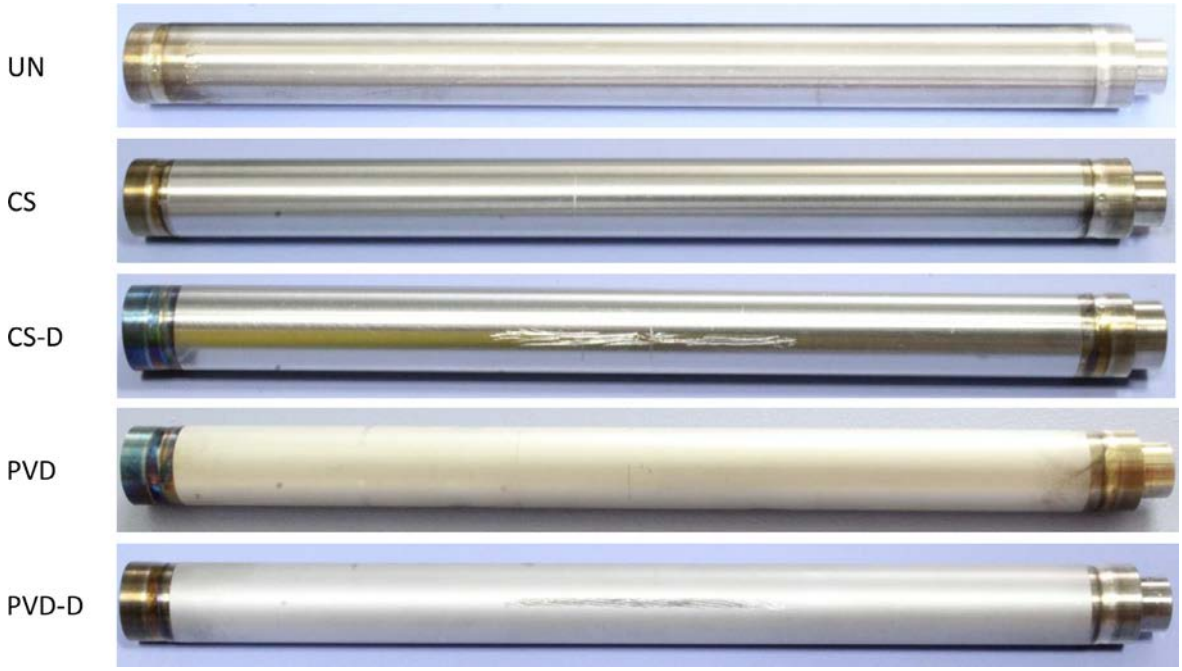

Fig. 1. Pre-test appearance of all sample types provided by WEC. UN=uncoated Optimized ZIRLO, CS=cold spray, PVD=magnetron sputtered, D=pre-damaged.

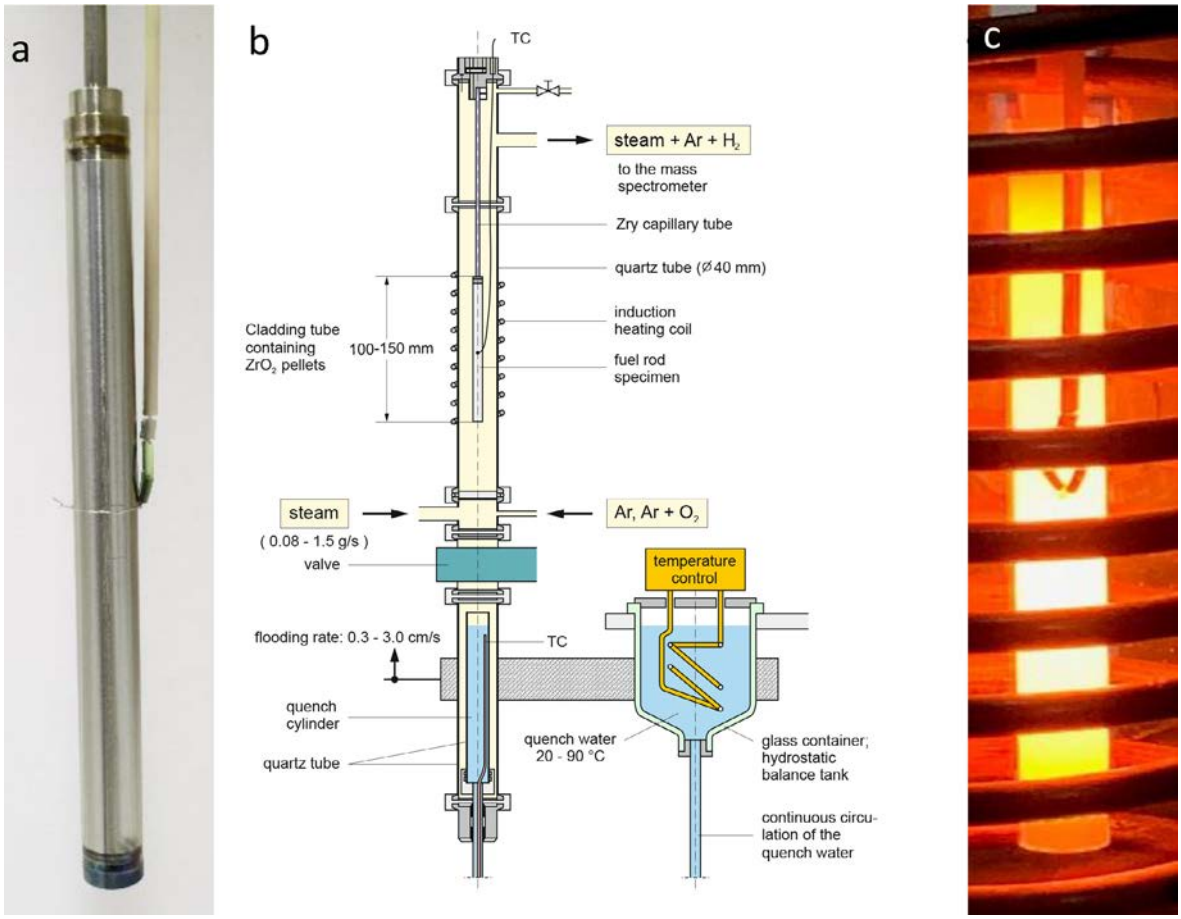

Fig. 2. (a) Pre-test sample, (b) Scheme of the QUENCH-SR facility, and (c) inductively heated sample in quartz glass surrounded by copper coil

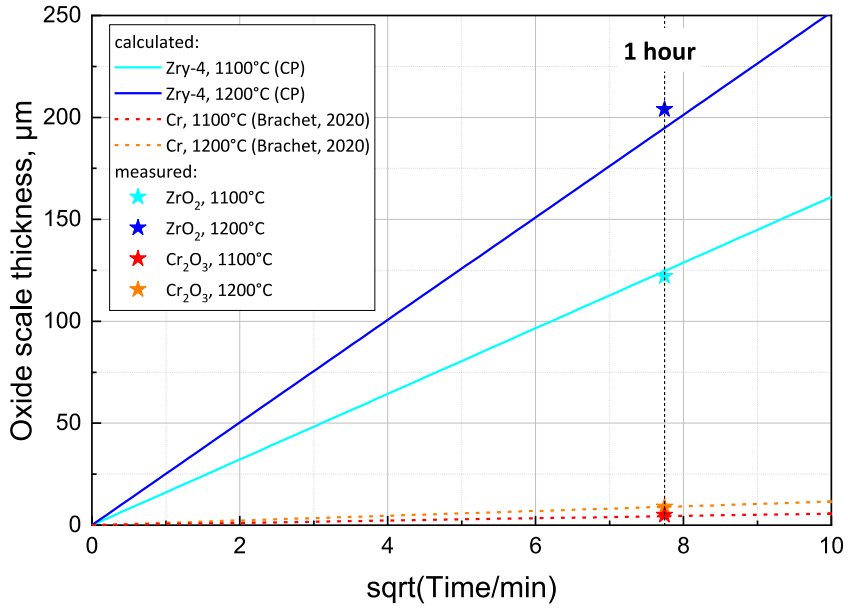

Fig. 3. Calculated thicknesses of ZrO_2 and Cr_2O_3 at 1100 and 1200 °C based on correlations from Cathcart/Pawel for Zry-4 ([24], taken from [25]) and Brachet et al. for Cr coatings [5], and measured values.

conducted with Cr-coated Zr alloy tubes (commercial standard PVD coating) including a thermocouple inside the empty specimens. These tests showed that the inner TC followed the pyrometer signal rather than the surface TC signal. That is why the sample temperature in the experiments described here was controlled by the pyrometer; whereas the surface TC provided an additional temperature signal. The comparison between the experimentally obtained oxide thicknesses with calculated values using well-accepted correlations were in good agreement (Fig. 3) and gave confidence that the accuracy of the temperature measurement by pyrometer at least in the isothermal tests presented here was better than ±20 K. At very high temperatures, which are reached in the transient tests with high oxide thicknesses, a stronger temperature gradient between the inner clad metal layer (which is heated by the induction system) and the outer oxide layer surface (where the temperature measurement takes place) must be expected.

Gas supply is controlled by Bronkhorst® gas flow controller, water flow controller and a CEM (controlled evaporator and mixer). 40 l/h argon flow through the facility throughout all tests, 60 g/h steam are injected during the oxidation phases resulting in a water steam concentration of 65 vol%.

Quenching by water is done with the lifting of a quartz cylinder filled with water at 95 °C and a quench rate of approx. 1 cm/s. The water level in the quench cylinder is kept constant by simultaneously raising a water storage tank containing a water heater, which is connected to the quench cylinder. The sample heating was shut off when the water level reached the bottom of the sample. Fig. 2b, c provides details about the test facility and sample.

The off-gas line is connected to a mass spectrometer (IPI GAM 3000) for quantitative measurement of steam, hydrogen, and other gases. The MS was calibrated for steam before the test series and regularly calibrated for hydrogen. The accuracy of the hydrogen concentration signal, used for analysis of the oxidation kinetics, is better than 5%.

From approx. 1200 °C in the transient tests and shortly before steam injection in the isothermal tests video recording started until the end of the experiments. Temperatures and gas flow in the facility are programmed by a dedicated LabView program, which also records data for pressure in the test section and power input.

Isothermal tests at 1100 and 1200 °C were conducted for one hour. The samples were heated at a rate of 1 K/s in inert atmosphere to the desired temperature, and steam flow was turned on approx. 2 min after the set temperature reached the isothermal plateau. All but one isothermal tests were terminated by water quenching. Transient tests were run with a heating rate of 10 K/min until failure of the sample. Steam was switched on at 800 °C. Failure criteria were escalation of hydrogen release rate (i.e. oxidation rate) beyond 10 vol.% in the off-gas or complete oxidation of the sample thus losing the capability of inductive coupling, which was observed by darkening of the middle part of the samples. Cooling of all samples in transient tests and one isothermally tested sample was in flowing argon with a high initial cooling rate of about 10 K/s down to 800 °C.

2.3. *Post-test examination*

The mass of the samples was determined before and (if possible) after test. The mass balance is provided in Table 1. It should be taken with care because (1) some samples broke during post-test handling, (2) some samples could not be separated from the suspension capillary, (3) oxide spalled off during the test or handling, and (4) residual cooling liquid from the thread cutting may have remained in the inner volume of the tube.

The pre- and post-test appearance was documented non-destructively by photography (Canon EOS 1200D) and SEM/EDX (Jeol 6100 with SiLi EDS detector or FEI XL30S with SDD EDS detector). The embedded samples were cut with a Struers Labotom cutting machine. The resulting cross-sections were embedded again, grinded and polished with a mild final etching.

The thicknesses of the oxide scales were measured with an optical microscope (OM) Reichert-Jung MeF3. A Leica DMi8 optical microscope was used for bright-field micrographs.

A FEI XL30S scanning electron microscope with silicon drift detector (SDD) was applied for EDS element analysis. Semi-quantitative EDS line-scans were done with an acceleration voltage of 15 kV at a device magnification of 5000x close to the surface of the samples (from epoxy inward).

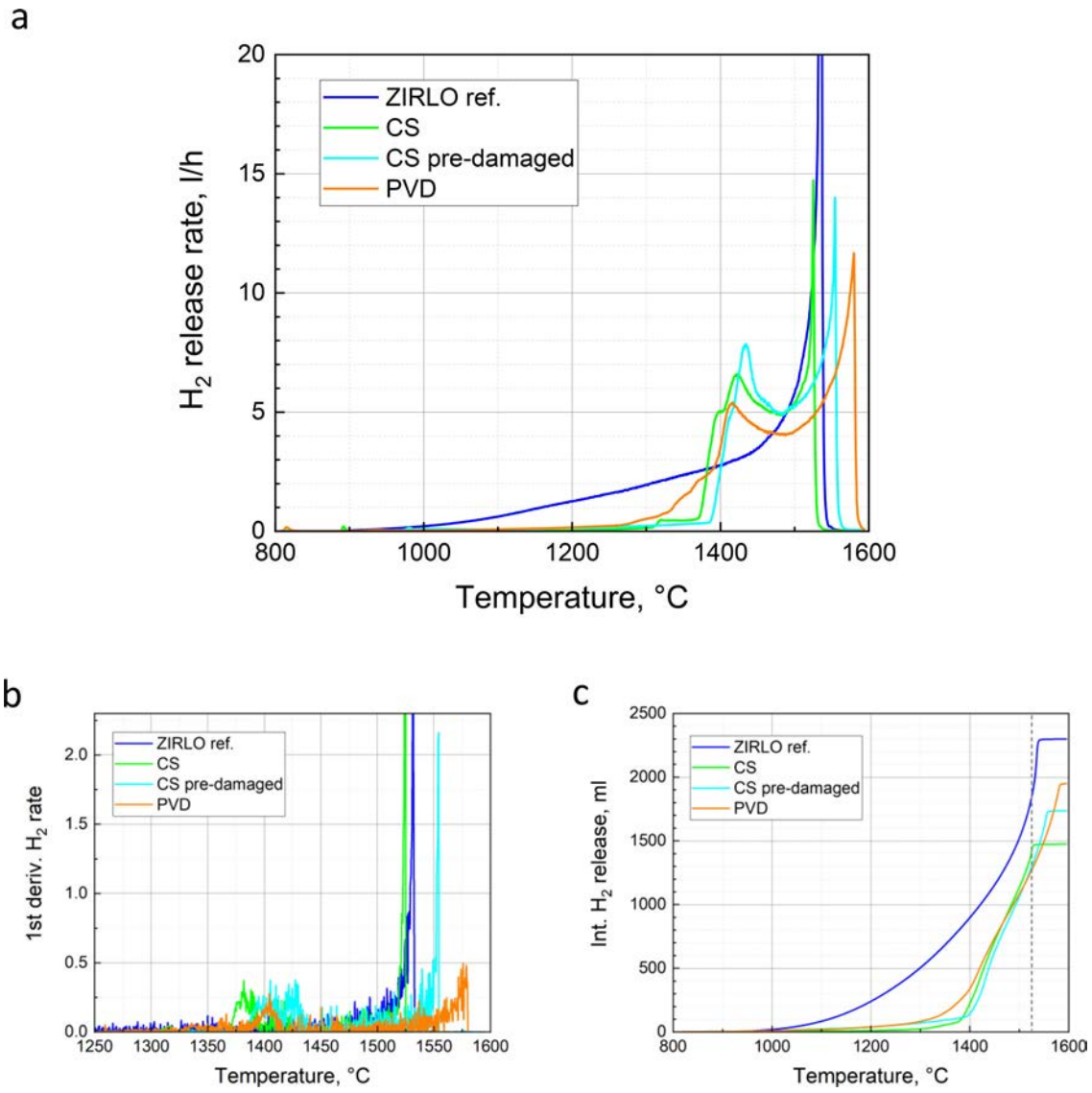

Fig. 4. Hydrogen release during transient tests: (a) release rates, (b) first derivatives above 1250 °C, (c) integral data.

3. Results

3.1. Online test data

The data obtained during the tests are summarized in Table 1 and Figs. 4 –6. A significant effect of the Cr coating became obvious for all test series. The mass change data given in Table 1 include the entire sample including the end plugs and, if indicated, the capillary suspension if it could not be separated from the sample.

3.1.1. Transient tests

Oxidation rates were significantly lower for the Cr-coated samples compared to the uncoated sample up to about 1350 ° for all coatings. As shown in Fig. 4, the failure temperature of the Cr-coatings (indicated by a significant increase of hydrogen release) is in the range 1350–1380 °C. The oxidation rates rapidly increased after failure for the cold-sprayed samples CS and CS-D, whereas the PVD sample showed a comparably slow increase of hydrogen release reaching comparable oxidation rates at about 1400 °C.

The oxidation rates of all coated samples became larger than the one of the uncoated sample soon after failure of the coatings at 1380...1400 °C. The oxidation rate of the uncoated sample increased continuously with rising temperature, whereas all coated samples showed a typical shape of the hydrogen release curves with a plateau between the first escalation after coating failure and the second escalation before termination of the experiments. The second escalation started at 1520...1550 °C with the lowest rates for the PVD coated sample, see first derivative curve in Fig. 4b. The switch-off criterion (approx. 10% H_2 in the off-gas) for the samples was reached between 1520 and 1580 °C with the order CS < UN < CS-D < PVD.

The variation between the hydrogen release signals of cold-sprayed samples with and without pre-damage seems not very significant. The integral hydrogen release of the pre-damaged sample at the same time and temperature shortly before the earliest termination of the test with the CS sample (1525 °C, as indicated by the gray dashed line in Fig. 4c) is even lower than for the non-scratched sample. Later on, it will be shown that the scratch into the Cr-coating of cold-sprayed samples only hardly reached the ZIRLO base material (Fig. 9). The integral hydrogen release of the coated samples at this time is significantly lower than of the uncoated reference sample as can be seen in Fig. 4 and Table 1. Generally, the data of the transient test series provided

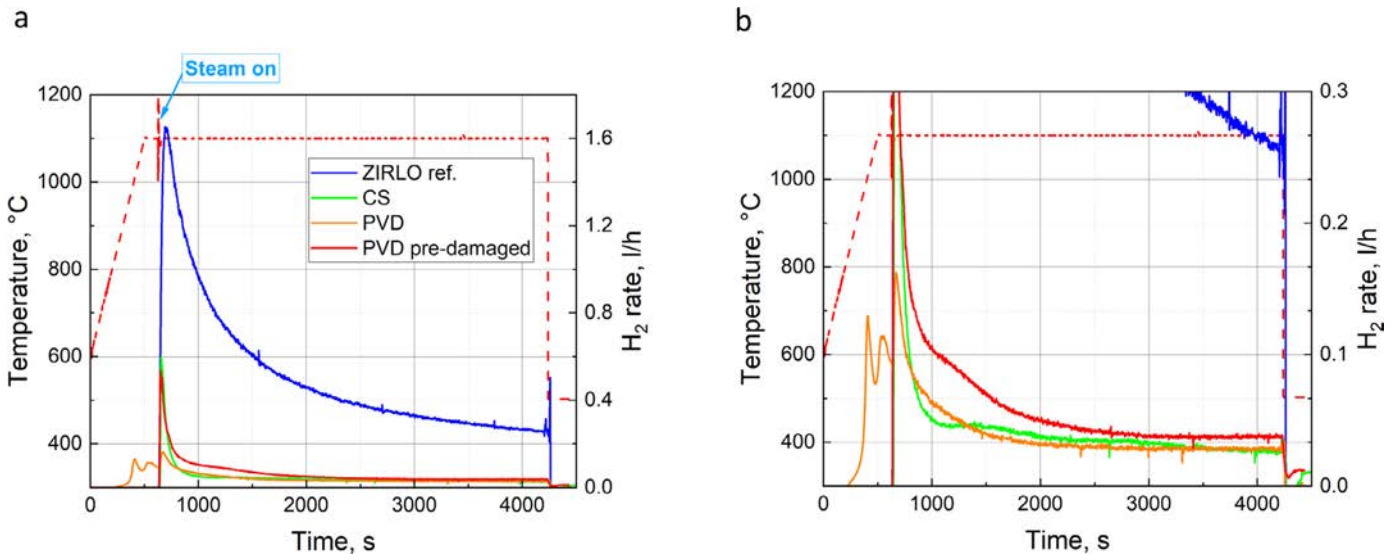

Fig. 5. Hydrogen release during isothermal tests at 1100 °C: (a) full scale, (b) magnified H_2 concentration scale.

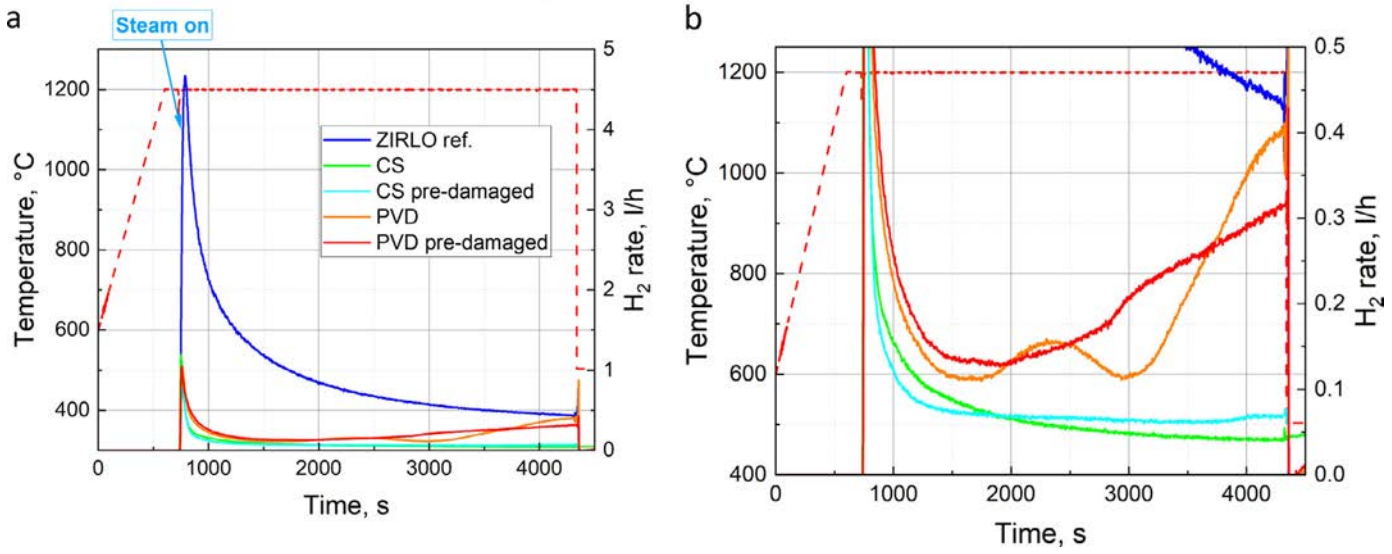

Fig. 6. Hydrogen release during isothermal tests at 1200 °C: (a) full scale, (b) magnified H_2 concentration scale.

in Table 1 (mass gain and H_2 release) look consistent, having in mind that the possibility for determination of the post-test mass was limited due to the strong oxidation and embrittlement of the samples.

3.1.2. Isothermal tests at 1100 °C

The data of the isothermal test series at 1100 °C show a significant protective effect of the coatings during the entire test duration, as seen in Fig. 5. The integral hydrogen released, and the mass gain of the coated samples are by more than one order of magnitude lower than of the uncoated sample, Table 1. Even though the oxidation of the PVD sample started already during the heat-up phase due to a minor technical problem (see remark in Table 1), the mass gain and the oxidation rates after 30 s in the isothermal oxidation phase are almost identical for the two undamaged samples (CS, PVD). The oxidation rate of the pre-damaged sample PVD-D is significantly higher during the first approx. 1000 s of oxidation and becomes more similar to the undamaged samples later on. This corresponds to the relatively large area of uncovered Optimized ZIRLO in the pre-damaged zone at the PVD-coated samples as seen in Fig. 9. Quenching with water of the uncoated, CS and PVD samples and fast cool-down in humid Ar flow of the PVD-D sample resulted in immediate termination of hydrogen release.

3.1.3. Isothermal tests at 1200 °C

The influence of the coating is also clearly visible for this test series at 1200 °C. In contrast to the series at 1100 °C, the two types of coating differ significantly, and the pre-damage has only a minor influence on hydrogen release. Fig. 6 shows reducing or constant hydrogen release throughout the 1 h test duration for the cold-sprayed samples. As for the test series at 1100 °C, the hydrogen release for these samples is by one order of magnitude lower compared to the uncoated sample; see also Table 1.

The thinner coatings PVD and PVD-D began to fail after 15…20 min in the isothermal phase resulting in a steadily increasing hydrogen release (i.e. oxidation rate) almost approaching the continuously decreasing hydrogen release rate of the uncoated sample after 60 min. This behavior is best seen in the magnified diagram, Fig. 6b. Note that the total hydrogen produced by the PVD samples was still much lower than for the uncoated cladding.

All tests of the 1200 °C series were terminated by water quenching, which resulted in a short and slight increase of the hy-

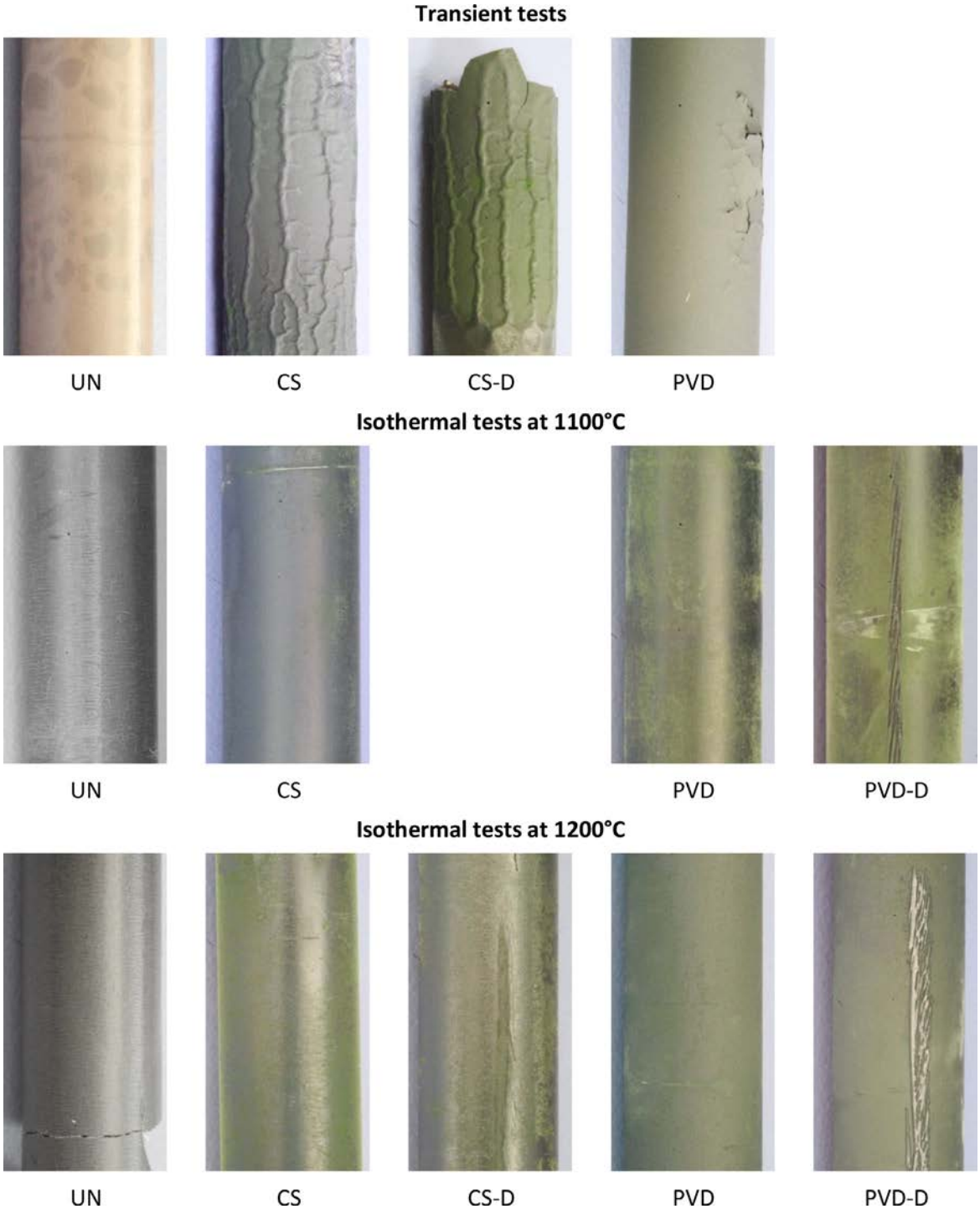

Fig. 7. Post-test appearance of samples, view of middle zones.

drogen signal for the PVD and uncoated samples and in an immediate termination of hydrogen production for the CS samples with protective coating until the end of the test.

3.2. Post-test examinations

3.2.1. Surface characterization

All samples were photographed after disassembling from the test rig. Fig. 7 shows images of the central region of all samples. All Cr-coated samples have a more or less greenish surface color from the chromium(III) oxide, Cr_2O_3, formed during oxidation by steam. The isothermally annealed samples had loose powdery green particles on the surface, which could be easily removed by wiping with a cloth. Apart from that, the surfaces of the isothermally treated samples were smooth.

By contrast, the surfaces of the samples after transient tests up to 1500…1600 °C look significantly changed with different appearance of the various sample types. The cold-sprayed samples CS and CS-D show a rippled surface with a network of embossed lines. According to the video recordings, these structures formed during the tests at around 1400–1450 °C. The (oxidized) coating of the PVD sample remained smooth, but partially flaked off. The spalling hap-

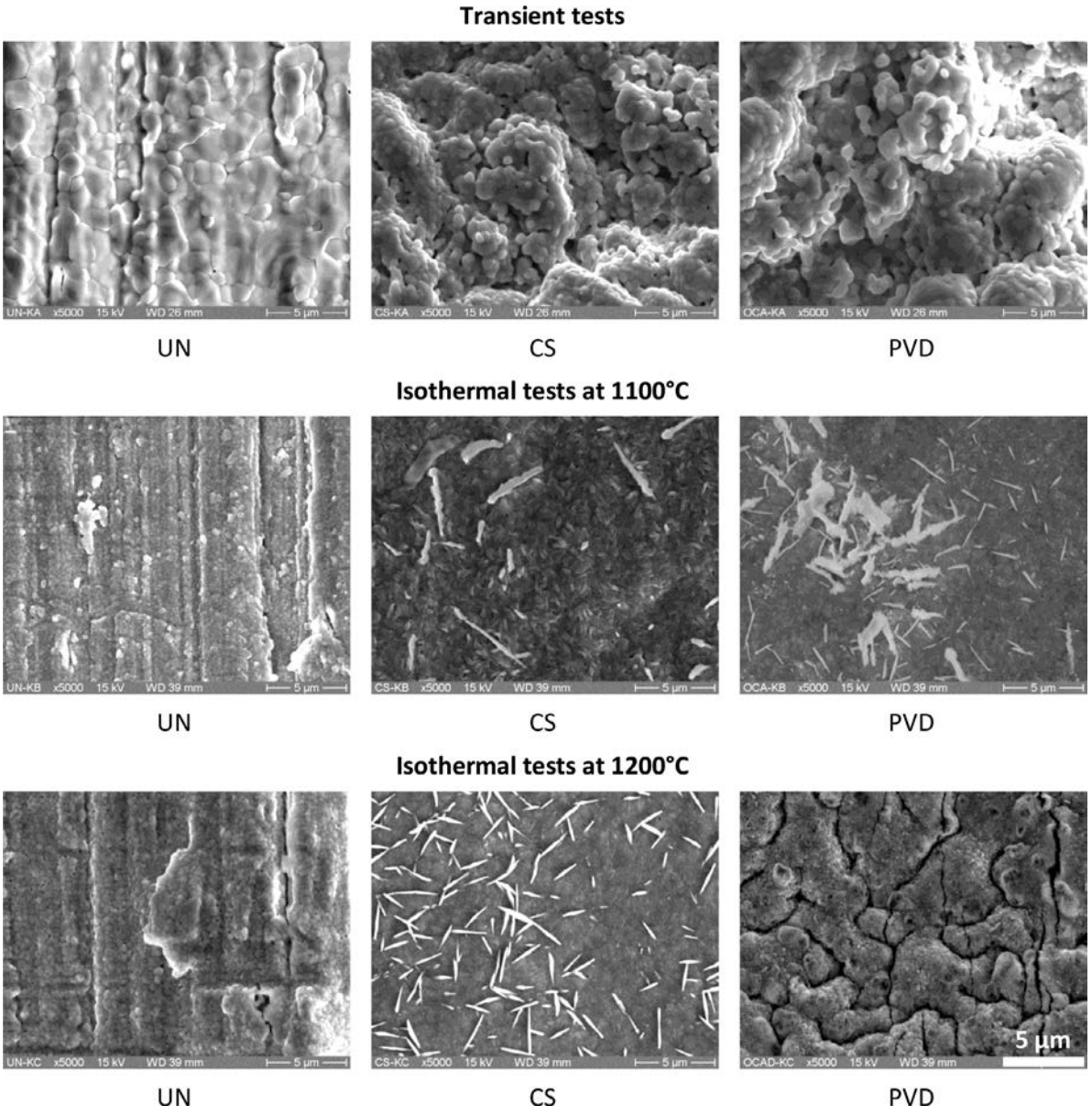

Fig. 8. SEM images of post-test sample surfaces.

pened only during the fast cooling phase as seen in the video. All samples after transient testing and the uncoated sample after the 1200 °C test were very brittle and broke partly during disassembly and post-test handling. The scratches of the pre-damaged samples are clearly visible also post-test, but seem not to be a source of coating failure in adjacent regions.

All sample surfaces were examined by SEM/EDX before embedding for metallography. Fig. 8 provides SEM images of the surfaces with the highest magnification (5000x). The zirconia (ZrO_2) scale on all three uncoated samples shows cracks mainly oriented in circumferential direction that were probably formed during fast cooling and quenching, respectively.

The surface of all Cr-coated samples looks more complex, consisting of round crystals, smooth areas and needle-like crystals, mainly found on these smooth areas. Semi-quantitative (standardless) EDX analysis of all these surface structures resulted in chromium oxide, at some places, mainly in valleys on the surface of the failed coatings, with minor ZrO_x content. Contrary to all other isothermally oxidized samples, the surface of the (failed) PVD sample shows a network of mainly intergranular, but also intragranular cracks.

Special attention was given to the scratched zones of the pre-damaged samples before and after the experiments. Fig. 9 gives typical examples of pre-damaged CS and PVD samples. The scratch on the thinner chromium coating prepared by PVD is through-going over a wide range of the pre-damaged zone as can be seen in the EDX line scan of that sample. On the other hand, the scratch in the cold sprayed coating goes only very locally through the Cr layer and reaches the ZIRLO base material. The oxidation of the uncovered Optimized ZIRLO surface seems to remain local, not affecting the surrounding Cr coated areas as can be seen from the SEM images and EDX line scans of the samples after testing.

3.2.2. Cross sections

All polished cross sections were analyzed by optical microscopy (OM). The OM micrographs were combined with results of SEM/EDX for determination of the layer structures after oxidation for each type of coating and temperature program.

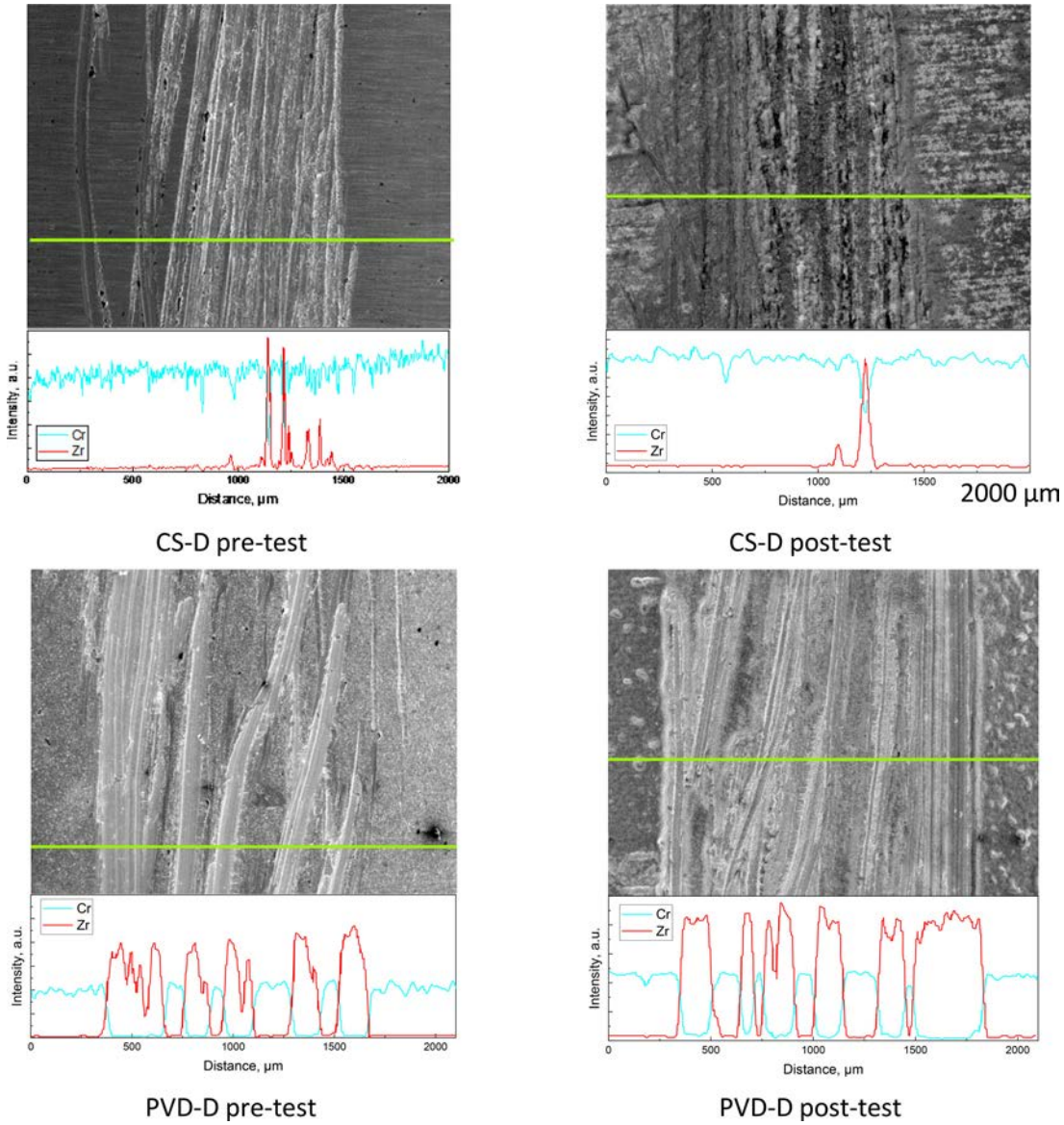

Fig. 9. SEM images and EDS line scans of scratches (pre-damage) on a cold-sprayed and a PVD Cr coating as received and after isothermal testing at 1200 °C.

Transient tests. The samples have been largely oxidized during the transient tests as seen in Fig. 10, with remaining of the oxidized chromium scale on top of a very thick zirconia region. Some oxygen-saturated metallic zirconium is left at the inner side of the cladding tubes. This region is also known to contain Cr for the coated samples, and generally other alloying elements, which are concentrated in the remaining metal phase [26].

Due to the different termination times/temperatures, a comparison between the tests is difficult, but the cold-sprayed samples show the comparably lowest degree of oxidation. A detachment of the chromia layer is partly visible for the cold-sprayed samples.

The outer part of the Zr oxide scale has a columnar structure. In the inner part of the oxide scale towards the metal-oxide interface, the Zr oxide is interspersed with metallic Zr phase. This is due to the dissociation of the cubic sub-stoichiometric ZrO_{2-x} phase, stable above 1520 °C, into stoichiometric tetragonal ZrO_2 and oxygen-saturated α-Zr(O) during cooling. This is a known effect of oxidation of Zr alloys at high temperatures beyond 1500 °C and corresponds to the Zr-O phase diagram [27,28].

Data of the layer thicknesses of all samples are provided in Table 2. Most coating thicknesses are average values of more or less scattered values. It could not be excluded that especially the hard and brittle chromia scales partly broke out during metallographic preparation of the samples.

Isothermal tests at 1100 °C. The uncoated sample looks as expected after one hour oxidation in steam with a thick zirconia layer and a layer of oxygen-stabilized α-Zr(O) underneath [29]. Cathcart/Pawel is a the name of a well-known correlation for the oxidation kinetics of Zr alloys [30], as seen in Fig. 6. The broken grains in the alpha-phase indicate its brittleness. The prior beta-phase with less oxygen content shows the typical Widmanstätten structure.

Both types of Cr coatings survived the 1 h oxidation at 1100 °C in steam, i.e., the Cr layers were only partly consumed by oxidation and interaction with the ZIRLO bulk, Fig. 11. The Cr oxide layer is about 30 times thinner than the Zr oxide on the uncoated sample. Zirconia with a comparable thickness to the uncoated sample formed locally at the bottom of the scratches, but did not affect the Cr coating in adjacent regions. The order of layers at all non-pre-damaged zones is Cr_2O_3/Cr/$ZrCr_2$/Zry as expected from literature [4,5,7] and former own experiments [9,26]. The intermetallic phase $ZrCr_2$ is around 1 µm thick for both sample types. The bulk Zr al-

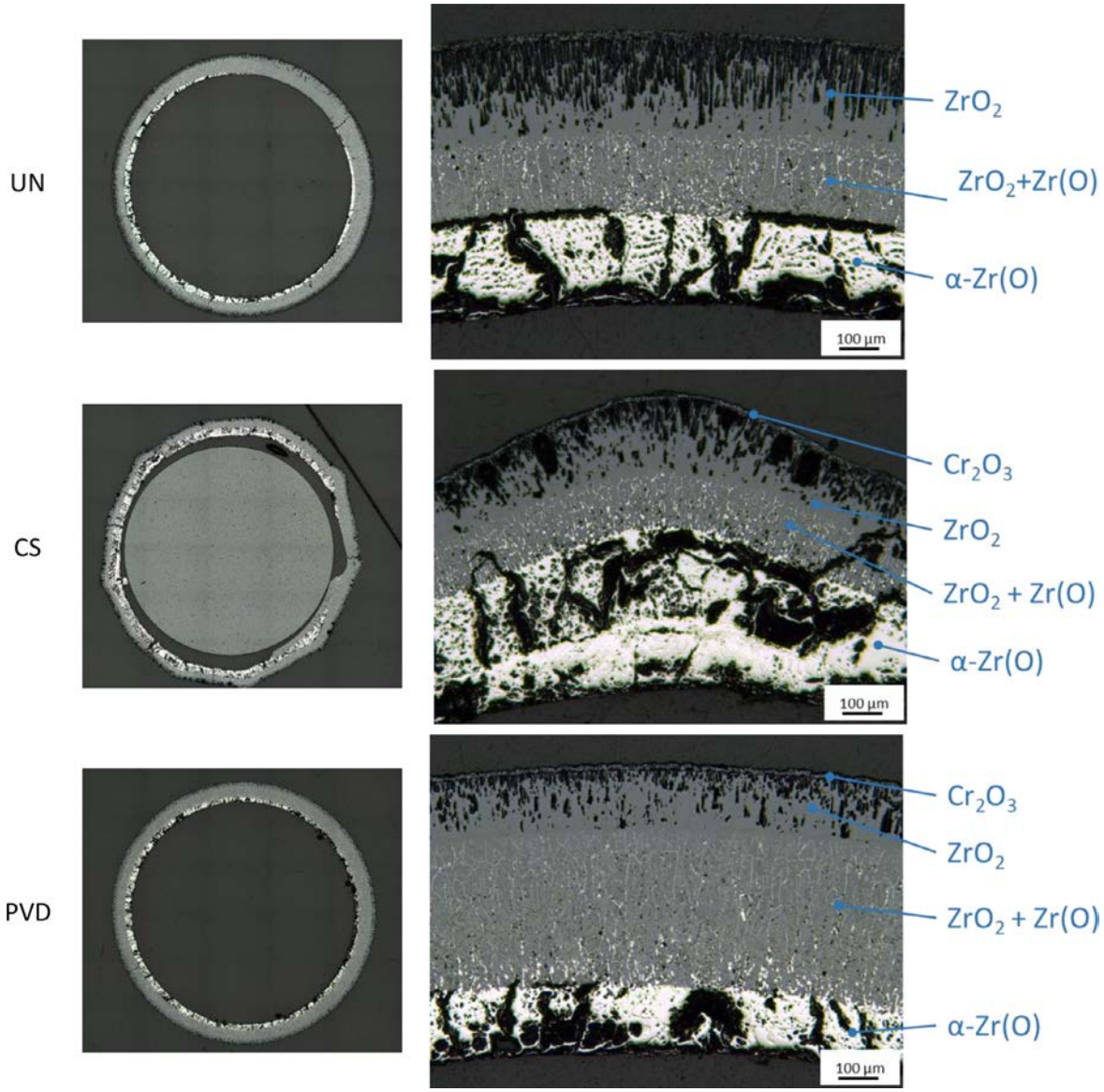

Fig. 10. Macrographs and OM micrographs of sample cross sections after transient tests.

loy was not converted to oxygen-stabilized α-Zr(O), i.e. the oxygen concentration in the bulk metal, which could not be quantitatively analyzed by EDS, remained below the solubility limit of the β-Zr phase of about 3 at% at 1100 °C [28].

Layer thicknesses of the middle cross sections are summarized in Table 2.

Isothermal tests at 1200 °C. The uncoated reference sample is also oxidized as expected after the 1200 °C test. The remaining prior beta-phase, which is the only ductile phase in the system, is comparably thin. The brittle sample broke during disassembly. This is the reason why oxide scale thickness provided in Table 2 could only be measured above and below the middle position.

Only the thicker cold-sprayed Cr coating withstood the 1 h oxidation at 1200 °C resulting in a partial oxidation of the chromium coating and the same order of layers like the samples at 1100 °C: Cr_2O_3/Cr/$ZrCr_2$/Zry, Fig. 12. The thickness of the $ZrCr_2$ phase between the coating and the bulk is around 1.5 µm. No oxygen ingress into the bulk Optimized ZIRLO was observed by means of OM and SEM/EDS.

As already seen in the hydrogen release curves with increasing oxidation rates after approx. 20 min, Fig. 6, the thinner PVD-coated Cr coating did not withstand the 1 h oxidation at 1200 °C. The micrographs show the formation of a relatively thick and non-homogeneous zirconia scale (max. 30 µm) below the Cr coating (but considerably thinner than at the uncoated sample). An around 3 µm thick dual phase layer consisting of $ZrCr_2$ and ZrO_2 is formed between the remaining Cr layer and the formed ZrO_2 phase. Beneath the Zr oxide, a 100-130 µm thick oxygen-stabilized α-Zr(O) phase (much thicker than the oxide layer) is observed. $ZrCr_2$ precipitations are seen in the bulk only in this phase.

A magnified view of the external part of the coated cladding reveals ZrO_2 veins through the Cr coating offering diffusion paths for oxygen from the ambient atmosphere to the Zry bulk, Fig. 13. The O area mapping is not shown in this picture, because it is not very meaningful due to an overlap of the Cr-L_α and O-K_α lines in the EDS spectra. Zr diffusion along the Cr grain boundaries was also found in the CS sample tested at 1200 °C, but these Zr veins did not pass through the Cr layer and therefore did not provide pathways for enhanced oxygen diffusion into the bulk.

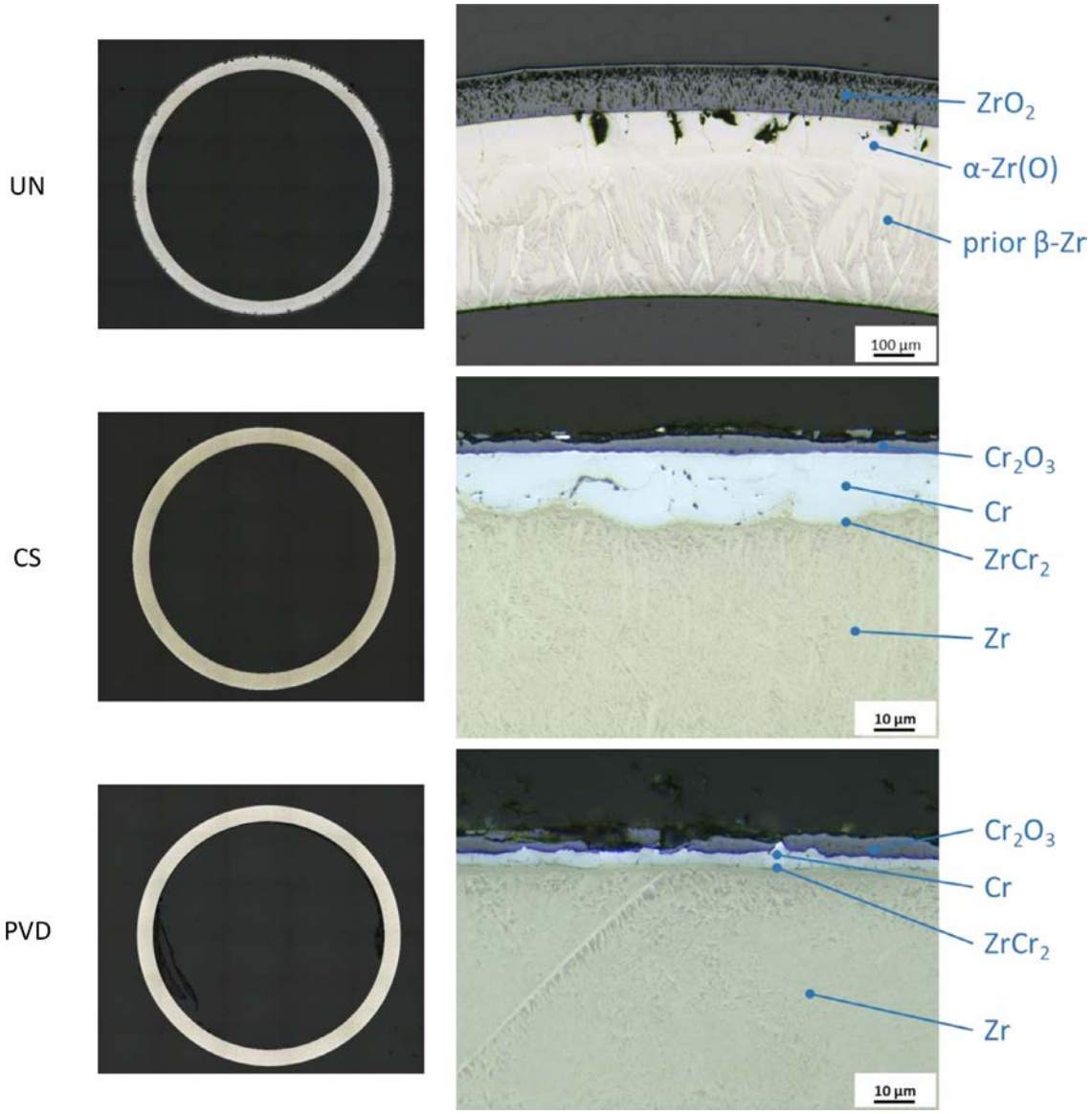

Fig. 11. Macrographs and OM micrographs of sample cross sections after isothermal tests at 1100 °C.

Behavior of pre-damaged Cr coating. As already seen in the hydrogen release curves and the surface examinations, the scratches applied to the specimens prior to the oxidation tests seem to have only a limited effect on the integral behavior of the samples. The effect of the scratch on the CS-D sample during the transient test up to very high temperature was "overwritten" by the strong, almost complete oxidation of the cladding tube. The position of the scratches was still visible at the surface, but not in the micrographs of the cross section.

The effect of scratches on the post-test appearance after testing at moderate temperatures should be discussed exemplarily for the PVD-D sample after the isothermal test at 1100 °C, Fig. 14. At places where the scratches reached the ZIRLO bulk, the ZrO_2 was formed locally according to the diffusion from this point/line source for the ingress of oxygen. The Zr oxide is observed also underneath adjacent Cr coating to a certain extent but did not cause spalling or other damage of the coating as can be seen in Fig. 14. The same behavior was observed for the pre-damaged sample CS-D after oxidation at 1200 °C. The PVD-D sample with partial failure of the Cr coating showed a transition from thinner ZrO_2 layers underneath the non-damaged region to thicker Zr oxide at the location of the scratches. Again, no sign of spalling or other damage of the Cr layer was observed.

4. Discussion

Both types of Cr coated samples showed significantly improved high-temperature corrosion resistance in steam up to the coating degradation/failure temperature compared to the uncoated samples under all tested conditions. The coating thickness seems to play a greater role in the oxidation behavior than the type of coating. In contrast to the PVD-coatings, the thicker cold-sprayed coatings survived the 1 h oxidation at 1200 °C and remained intact longer and up to higher temperatures during the transient tests.

A typical shape of hydrogen release curves, i.e. oxidation rates, was found for all coated samples in the transient test series with two maxima and a pronounced valley in-between. The failure of the Cr-coating results in the first peak in oxidation rate, which caused fast formation of ZrO_2 on the then unprotected surface. The growing dense zirconia scale provides some degree of protection and is responsible for the valley. The phase transition from tetragonal to cubic zirconia at T>1500 °C with the corresponding increase

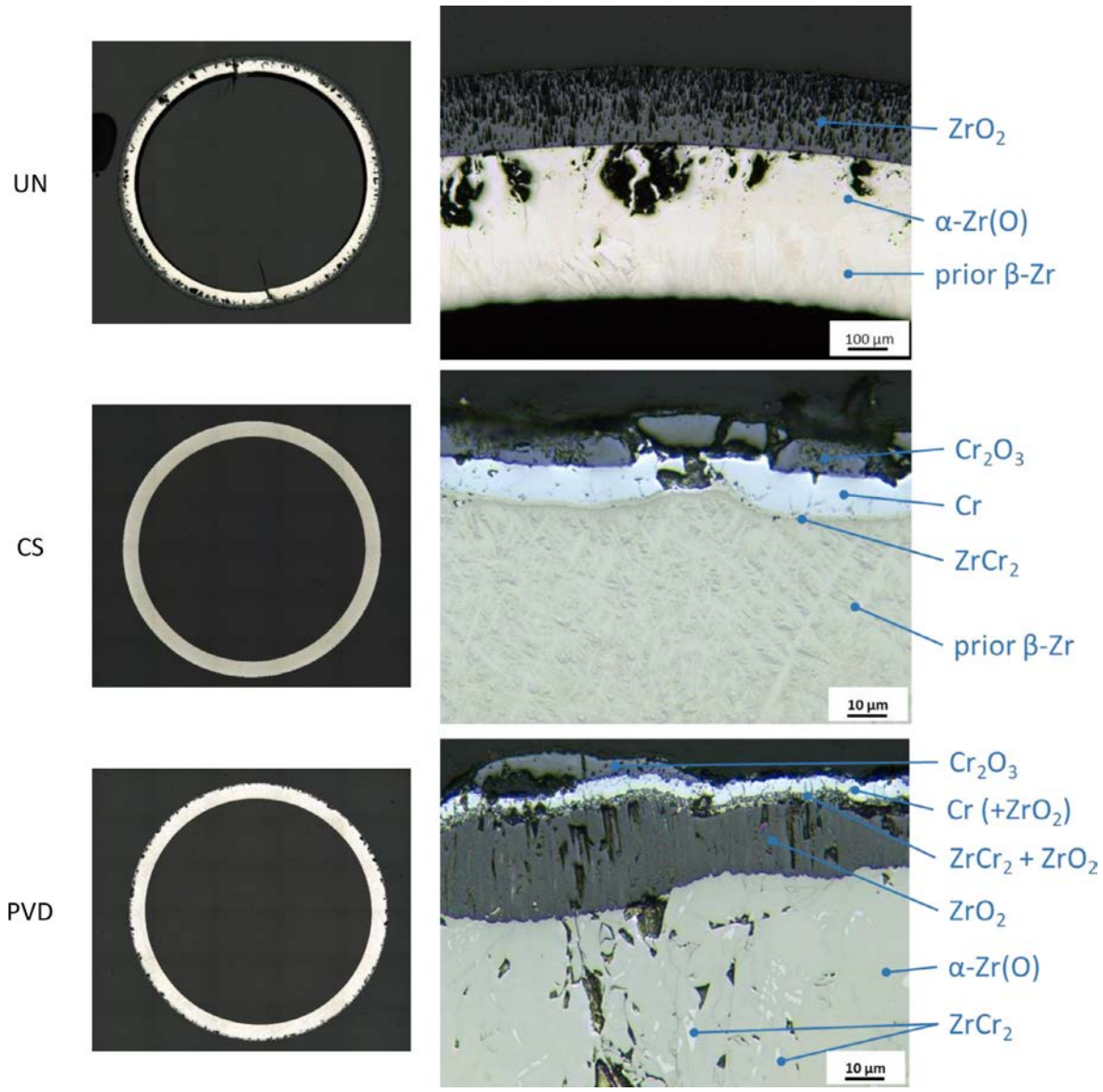

Fig. 12. Macrographs and OM micrographs of sample cross sections after isothermal tests at 1200 °C.

in oxygen diffusion coefficient in the oxide and, with it, of the oxidation rate is responsible for the second runaway before termination of the experiments.

This hypothesis for the behavior during the transient experiments was confirmed by a dedicated test series with termination of the oxidation after different times and at different temperatures [26]. Zircaloy-4 plate samples coated with 14 µm PVD Cr layer were oxidized in steam using a tube furnace with well-defined boundary conditions. The temperature program with 10 K/min heating rate was identical to the test series presented here. The heating phase was stopped at 1200, 1300, 1350, 1400, 1500, 1550, and 1600 °C. The oxidation kinetics with two pronounced peaks, here also analyzed by online MS measurements of the hydrogen release, were very similar to this test series. Detailed post-test examinations investigations led to the following conclusions regarding the degradation mechanism of the Cr coating [26]:

Stage 1: Oxidation of the Cr coating and the formation of a protective dense Cr_2O_3 scale and inter-diffusion between Cr coating and Zr substrate.

Stage 2: Degradation of the dense structure of the outer protective Cr_2O_3 scale by the reaction between Zr and Cr_2O_3, diffusion of Zr along the Cr grain boundaries and its oxidation, later on, the Zr–Cr eutectic reaction, and potentially volatilization of Cr_2O_3. The ZrO_2 veins along grain boundaries in the metallic Cr coating provide oxygen diffusion paths. Eventually, coating failure occurs, and oxygen diffuses massively into the substrate causing its extensive oxidation.

Stage 3: Formation of a dense columnar Zr oxide layer acting as a moderately effective oxygen diffusion barrier, which decreases the oxidation rate and reduces the hydrogen release even with increasing temperatures.

Stage 4: Transformation of tetragonal ZrO_2 to more substoichiometric cubic ZrO_{2-x} at T>1500 °C, leading to the transition of dense columnar grains to bulk equiaxed grains with cracks and an increased oxygen diffusion coefficient in the zirconia layer. Consequently, the release of hydrogen is accelerated again.

Table 2
Main layer thicknesses measured at OM cross sections.

Sample	Axial Position, mm	Layer	Mean thickness, µm	Remarks
UN trans	50 mm	Zr oxide	611 ± 122	
CS trans	< 50 mm	Zr oxide	434 ± 163	Incl. ca. 10 µm Cr_2O_3
CS-D trans	50 mm	Zr oxide	498 ± 65	Incl. ca. 10 µm Cr_2O_3
PVD trans	50 mm	Zr oxide	555 ± 61	Incl. ca. 15 µm Cr_2O_3
UN 1100 °C	50 mm	Zr oxide	122 ± 3	
CS 1100 °C	50 mm	Cr oxide	4	
		Cr metal	15	
PVD 1100 °C	50 mm	Cr oxide	4	
		Cr metal	4	
PVD-D 1100 °C	50 mm	Cr oxide	5	
		Cr metal	5	
UN 1200 °C	40 mm	Zr oxide	204 ± 6	
UN 1200 °C	70 mm	Zr oxide	183 ± 2	
CS 1200 °C	50 mm	Cr oxide	10	Crumbly layer, perhaps originally thicker
		Cr metal	15	
CS-D 1200 °C	50 mm	Cr oxide	10	Crumbly layer, perhaps originally thicker
		Cr metal	16	
PVD 1200 °C	50 mm	Cr oxide	0–10	Not continuous, partly with bubbles
		Cr metal	5	Interspersed with oxide
		Zr oxide	0-30	Island-shaped
PVD-D 1200 °C	50 mm	Cr oxide	0-3	Crumbly layer, perhaps originally thicker
		Cr metal	8	Interspersed with oxide
		Zr oxide	0-8	Island-shaped
		α-Zr(O)	100-130	

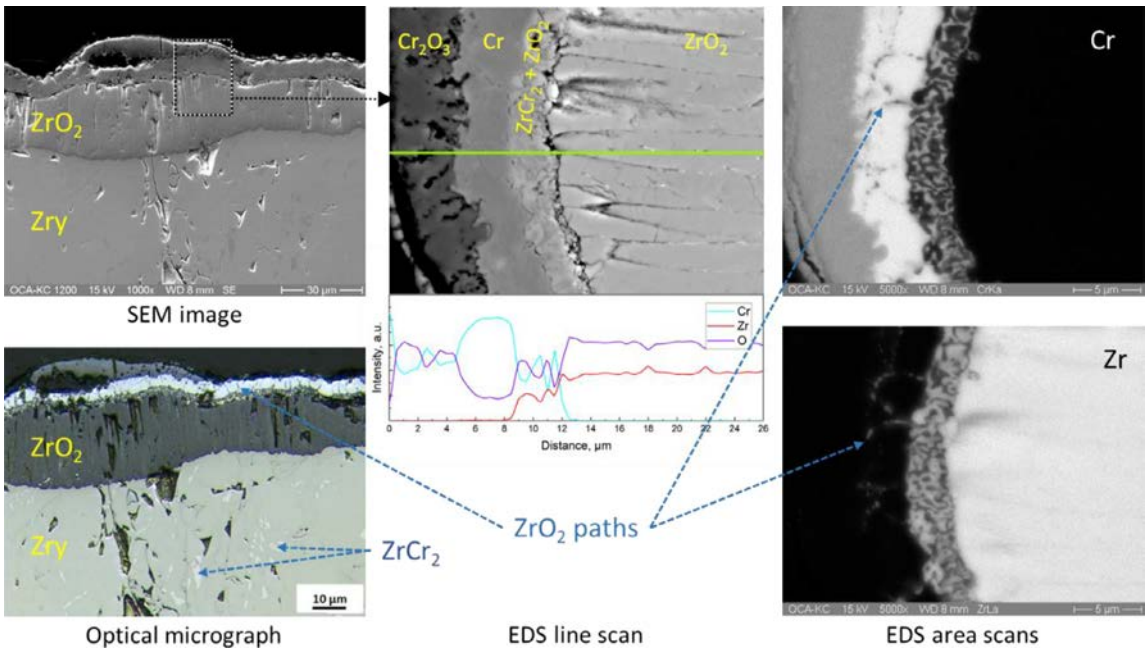

Fig. 13. Magnified view on the coating of PVD sample after isothermal oxidation at 1200 °C.

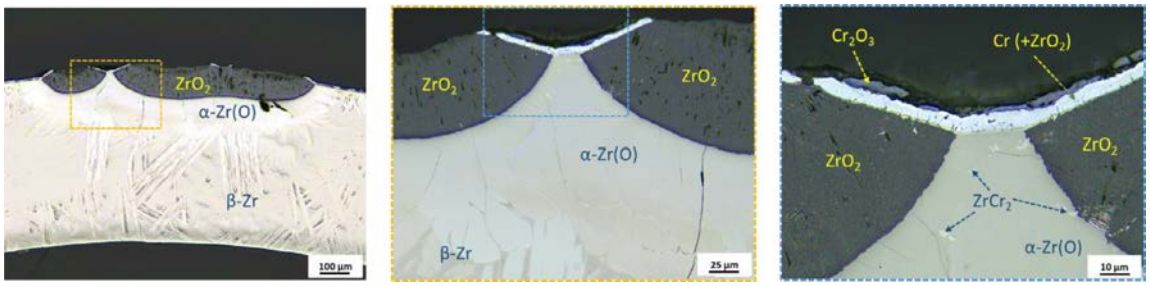

Fig. 14. OM micrographs of the pre-damaged PVD sample after isothermal oxidation at 1100 °C with three different magnifications.

These four stages agree well and could be directly applied to the transient test series of this study with only one sample per test condition. A fifth stage with a third hydrogen peak was observed in Liu's tests [26] at the highest maximum temperatures of 1550 and 1600 °C, when the samples broke and steam got access to the remaining metallic parts in the center of the plate samples oxidized from both sides. This step was not reached in transient tests of this study with maximum temperatures of 1520 and 1580 °C and only one side oxidation, which by the way, is more prototypical.

The authors are aware that the chosen heating rate in the transient tests is not prototypical for accidents scenarios of LWRs and that faster transient may result in quantitatively different results, i.e. coating failure at higher temperatures. The heating rate of 10 K/min was chosen to be slow enough to give the diffusion and oxidation processes sufficient time to develop, on the one hand, and fast enough to avoid complete oxidation of the sample before the relevant temperatures were reached, on the other. The results presented here are not prototypical for LOCA scenarios, but should at least be rather conservative.

The CS samples during both isothermal tests and the PVD samples at 1100 °C remained in Stage 1 described above with the formation of a protective chromia scale and effective prevention of oxygen diffusion into the Optimized ZIRLO base material. Stage 2 was obviously reached for the PVD coated sample at 1200 °C. The formation of ZrO_2 precipitates along the Cr grain boundaries offered diffusion paths for oxygen ingress into the bulk Zr alloy. Zirconium-enriched grain boundaries in the Cr layer were also found in the thicker CS coating, but they did not pass through the Cr thickness (only up to 30–50% of the Cr layer from the original Cr/Zr interface). Interestingly, the thickness of the oxygen-stabilized α-Zr(O) phase is much thicker (100-130 µm) than the ZrO_2 layer ($<$ 30 µm) for the PVD sample tested at 1200 °C. This is an indication, that the oxidation kinetics was determined by the limited flow of oxygen through the partly degraded Cr coating similarly to the oxidation of Zr alloys in steam-starved conditions. The behavior of the PVD coating at 1200 °C with the formation of zirconia diffusion paths through the Cr scale resulting in a smooth transition from "protective" to "failed" coating also corresponds with the degradation mechanism described by Brachet et al. [5].

The different thickness of the both types of Cr coatings is probably also the reason for the different surface appearance of the samples after the transient tests. Due to the initial lower thickness of the PVD samples, most of the metallic Cr coating has been consumed (both by outer Cr_2O_3 oxide formation and by inner Cr diffusion into the clad substrate) and/or a zirconia layer has been formed (separating the remaining Cr coating from the Zry bulk) before reaching temperatures higher than the Zr-Cr eutectic one. On the other hand, for the thicker CS coating, there is likely a thick residual Cr metallic layer, which induce Zr-Cr eutectic reaction when reaching the higher temperatures resulting in the rippled surface. Such influence of the thickness of the initial Cr layer was recently discussed by Chaari et al. [31]. The micrographs of the samples after the isothermal tests at 1200 °C, Fig. 12, can illustrate possible initial conditions for both types of coatings when reaching the eutectic temperature.

All samples in isothermal tests survived quenching by preheated water. Brittle samples only broke post-test during disassembly or handling. There was no indication of delamination of the coatings by the water quenching procedure, which should result in extreme thermal stresses.

Volatilization of chromia, as described e.g. by Meschter et al. [22] and Opila [32] should have played no role during the isothermal tests at the moderate temperatures. Brachet et al. [5] discussed that the contribution of chromium volatilization could be neglected up to at least 1300 °C. CrO_x volatilization could not be excluded for the final part of the transient experiments at very high temperatures, but even then, it should not have significantly affected the oxidation kinetics, which at this stage is determined by the oxygen diffusion through the growing Zr oxide layer.

A positive result of this study for the application of Cr coated cladding tubes in LWRs is that pre-damage of the cladding e.g. by scratches seems to have only limited effect on the HT oxidation behavior of the cladding tubes. Oxidation and formation of zirconia was only found locally where the scratches were going through the coating. For both types of coatings, no adjacent regions were affected.

5. Summary and conclusion

A series of experiments with prototype commercial Cr-coated Optimized ZIRLO cladding tube segments were performed isothermally at 1100 and 1200 °C and with transient tests until the cladding tubes were almost completely oxidized. On the one hand, the positive effect of the coatings on the high-temperature oxidation resistance in steam was clearly demonstrated for all tested conditions. For coated samples, hydrogen release was measured to be more than an order of magnitude lower as long as the coating remained intact. In addition, the integral hydrogen release was lower for coated samples than for uncoated samples under all test conditions. On the other hand, the loss of the protective effect of the coatings at very high temperatures remains a problem for all applications of coated Zr alloy claddings. The positive feedback of higher oxidation rates leading to higher chemical energy release, as well as the larger amount of remaining Zr metal after coating failure, may lead to earlier and more intense temperature runaway compared to uncoated claddings at comparable times and temperatures. This needs to be tested in bundle tests, as envisaged in the OECD-NEA Joint Undertaking QUENCH-ATF [33], as well as simulated by SA computer codes with improved models for ATF materials, as is being done, for example, in the ongoing IAEA project ATF-TS [34] and the upcoming OECD-NEA project TCOFF-2.

The thickness of the Cr layers appears to have the greatest influence on the protective effect of the coating. In addition to the known degradation mechanisms for the Cr coating (oxidation, diffusion of Cr into the Zry bulk, volatilization at very high temperatures), the grain boundary diffusion of Zr into the Cr coating seems to be another essential mechanism for the loss of the protective effect of the coating. For the application as nuclear fuel cladding tube, a compromise for an optimal Cr thickness has to be found, taking into account e.g. the desired protective effect, neutronic penalties and production costs. The Cr coating thicknesses used in this study should be appropriate for application as an ATF cladding tube.

Pre-damage of the coating, e.g. by scratches, only locally led to increased oxidation and does not seem to be a major problem for the application. The adhesion of the Cr coating to the ZIRLO material was excellent for both coating types. Even extreme thermal stresses during water quenching from 1100 and 1200 °C did not cause spalling.

The ultimate upper limit for the protective effect of Cr coatings, i.e. the eutectic temperature at 1332 °C, can be shifted to higher temperatures by applying a diffusion barrier layer between the Cr coating and the base material. Promising approaches with ceramic (CrN, ZrO_2, ...) and metallic (Nb, Mo, Ta, ...) diffusion barriers are under development worldwide. The advantages and disadvantages of the different approaches are discussed in the recent review papers by Kashkarov et al. [3] and Yang et al. [14].

Declaration

This paper was prepared as an account of work partly sponsored by an agency of the United States Government. Neither the

United States Government nor any agency thereof, nor any of their employees, makes any warranty, express or implied, or assumes any legal liability or responsibility for the accuracy, completeness, or usefulness of any information, apparatus, product, or process disclosed, or represents that its use would not infringe privately owned rights. Reference herein to any specific commercial product, process, or service by trade name, trademark, manufacturer, or otherwise does not necessarily constitute or imply its endorsement, recommendation, or favoring by the United States Government or any agency thereof. The views and opinions of authors expressed herein do not necessarily state or reflect those of the United States Government or any agency thereof.

Declaration of Competing Interest

The authors declare that they have no known competing financial interests or personal relationships that could have appeared to influence the work reported in this paper.

CRediT authorship contribution statement

M. Steinbrück: Conceptualization, Methodology, Investigation, Writing – original draft. **U. Stegmaier:** Investigation, Writing – review & editing. **M. Große:** Investigation, Writing – review & editing. **L. Czerniak:** Resources, Writing – review & editing. **E. Lahoda:** Resources, Writing – review & editing. **R. Daum:** Conceptualization, Writing – review & editing, Funding acquisition. **K. Yueh:** Writing – review & editing.

Acknowledgments

This work was conducted in the framework of a bilateral contract between WEC and KIT.

The samples were supplied by work supported by the Department of Energy under Award Number DE-NE0008824.

At KIT, the work was conducted in the framework of the HGF program NUSAFE.

References

[1] K. Terrani, Accident tolerant fuel cladding development: promise, status, and challenges, J. Nucl. Mater. 501 (2018) 13–30.
[2] C. Tang, M. Stueber, H. Seifert, M. Steinbrueck, Protective coatings on zirconium-based alloys as accident-Tolerant fuel (ATF) claddings, Corros. Rev. 35 (2017) 141–165.
[3] E. Kashkarov, B. Afornu, D. Sidelev, M. Krinitcyn, V. Gouws, A. Lider, Recent advances in protective coatings for accident tolerant zr-based fuel claddings, Coatings 11 (2021) 557 art. no..
[4] J.C. Brachet, I. Idarraga-Trujillo, M. Flem, M. Saux, V. Vandenberghe, S. Urvoy, E. Rouesne, T. Guilbert, C. Toffolon-Masclet, M. Tupin, C. Phalippou, F. Lomello, F. Schuster, A. Billard, G. Velisa, C. Ducros, F. Sanchette, Early studies on Cr–coated zircaloy-4 as enhanced accident tolerant nuclear fuel claddings for light water reactors, J. Nucl. Mater. 517 (2019) 268–285.
[5] J.C. Brachet, E. Rouesne, J. Ribis, T. Guilbert, S. Urvoy, G. Nony, C. Toffolon-Masclet, M.Le Saux, N. Chaabane, H. Palancher, A. David, J. Bischoff, J. Augereau, E. Pouillier, High temperature steam oxidation of chromium-coated zirconium-based alloys: kinetics and process, Corros. Sci. 167 (2020) 108537 art. no..
[6] X. Han, J. Xue, S. Peng, H. Zhang, An interesting oxidation phenomenon of Cr coatings on Zry-4 substrates in high temperature steam environment, Corros. Sci. 156 (2019) 117–124.
[7] X. Han, C. Chen, Y. Tan, W. Feng, S. Peng, H. Zhang, A systematic study of the oxidation behavior of Cr coatings on Zry4 substrates in high temperature steam environment, Corros. Sci. 174 (2020) 108826 art. no..
[8] X. Hu, C. Dong, Q. Wang, B. Chen, W.T.H. Yang, R. Zhang, W. Gu, D. Chen, High--temperature oxidation of thick Cr coating prepared by arc deposition for accident tolerant fuel claddings, J. Nucl. Mater. 519 (2019) 145–156.
[9] E. Kashkarov, D. Sidelev, M. Syrtanov, C. Tang, M. Steinbrück, Oxidation kinetics of Cr-coated zirconium alloy: effect of coating thickness and microstructure, Corros. Sci. 175 (2020) 108883 art. no..
[10] J. Krejčí, L. Cvrček, P. Šutta, P. Bublíková, M. Ševeček, J. Kabátová, J. Kočí, F. Manoch, P. Halodová, H. Namburi, J. Málek, S. Krum, Experimental behaviour of chromium based coatings, in: Proceedings of the TOP FUEL 2018 Conference, Prague, Czech Republic, 2018 30 Sept-04 Oct 2018.
[11] H. Yeom, B. Maier, G. Johnson, T. Dabney, M. Lenling, K. Sridharan, High temperature oxidation and microstructural evolution of cold spray chromium coatings on zircaloy-4 in steam environments, J. Nucl. Mater. 526 (2019) 151737 art. no..
[12] H.B. Ma, J. Yan, Y.H. Zhao, T. Liu, Q.S. Ren, Y.H. Liao, J.D. Zuo, G. Liu, M.Y. Yao, Oxidation behavior of Cr-coated zirconium alloy cladding in high-temperature steam above 1200°C, NPJ Mater. Degrad. 5 (2021) 7 art. no..
[13] C. Tang, M. Grosse, M. Steinbrueck, K. Shirvan, Oxidation and quench behavior of cold spraying Cr-coated zircaloy fuel cladding under severe accident scenarios, in: Proceedings of the International Nuclear Fuel Cycle Conference and TOP FUEL 2019 - Light Water Reactor Fuel Performance Conference, 2020.
[14] J. Yang, M. Steinbrück, C. Tang, M. Große, J. Liu, J. Zhang, D. Yun, S. Wang, Review on chromium coated zirconium alloy accident tolerant fuel cladding, Rev. Chromium Coat. Zircon. Alloy Accid. Toler. Fuel Cladding 895 (2022) 162450 art. no..
[15] K. Pasamehmetoglu, State-of-the-Art Report on Light Water Reactor Accident–Tolerant Fuels, OECD-NEA, Paris, 2018.
[16] K. Geelhood, W. Luscher, Degradation and Failure Phenomena of Accident Tolerant Fuel Concepts. Chromium Coated Zirconium Alloy, Pacific Northwest National Laboratory, Richland, Washington, 2019.
[17] H. Okamoto, Cr-Zr (chromium-zirconium), J. Phase Equilib. 14 (1993) 768.
[18] J. Yang, T.C.U. Stegmaier, M. Steinbrück, W.S.M. Große, H. Seifert, High temperature Cr-Zr interaction of two types of Cr-coated Zr alloys in inert gas environment, J. Nucl. Mater. 547 (2021) 152806 art. no..
[19] J.C. Brachet, M. Dumerval, H. Palancher, J. Bischoff, E. Pouillier, Behavior of Chromium coated m5 claddings upon thermal ramp tests under internal pressure (loss-of-coolant accident conditions), in: Proceedings of the TOP FUEL 2018 Conference, 2018 Prague, Czech Republic, 30 Sept-04 Oct 2018.
[20] N. Birks, G. Meier, F. Pettit, Introduction to the High Temperature Oxidation of Metals, 2nd ed., Cambridge University Press, 2006.
[21] M. Stanislowski, E. Wessel, K. Hilpert, T. Markus, L. Singheiser, Chromium vaporization from high-temperature alloys, J. Electrochem. Soc. 154 (2007) A295–A306.
[22] P. Meschter, E. Opila, N. Jacobson, Water vapor-mediated volatilization of high--temperature materials, Ann. Rev. Mater. Res. 43 (2013) 559–588.
[23] P. Hofmann, V.V. Noack, M. Veshchunov, A. Berdyshev, A. Boldyrev, L. Matweev, A. Palagin and V. Shestak, "Physico-chemical behaviour of zircaloy fuel rod cladding tubes during LWR severe accident reflood. part i: experimental results of single rod quench experiments. Part ii: modelling of quench phenomena," Report FZKA-5846, 1997, Forschungszentrum Karlsruhe, Germany.
[24] J. Cathcart, R. Pawel, R. McKee, R. Druschel, G. Yurek, J. Campbell, S. Jury, Zirconium Metal-Water Oxidation Kinetics IV. Reaction Rate Studies, ORNL, USA, 1977 ORNL/NUREG-17,.
[25] G. Schanz, B. Adroguer, A. Volchek, Advanced treatment of zircaloy cladding high-temperature oxidation in severe accident code calculations part i. Experimental database and basic modeling, Nucl. Eng. Des. 232 (2004) 75–84.
[26] J. Liu, C. Tang, M. Steinbrück, J. Yang, U. Stegmaier, M. Große, D. Yun, H. Seifert, Transient experiments on oxidation and degradation of Cr-coated Zircaloy in steam up to 1600°C, Corros. Sci. 192 (2021) 109805 art. no..
[27] M. Steinbrück, M. Grosse, Deviations from parabolic kinetics during oxidation of zirconium alloys, ASTM Spec. Tech. Publ. STP 1543 (2015) 979–1001.
[28] T. Massalski, H. Okamoto, P. Subramanian, L. Kacprzak, Binary Alloy Phase Diagrams, ASM International, 1990.
[29] vol. 1 M. Steinbrück, High-temperature oxidation of zirconium alloys in various atmospheres, in: F.G. Caballero (Ed.), Encyclopedia of Materials: Metals and Alloys, Elsevier, Oxford, 2022, pp. 454–463. vol. 1.
[30] R. Pawel, J. Cathcart, R. McKee, The kinetics of oxidation of zircaloy-4 in steam at high temperatures, J. Electrochem. Soc. 126 (1979) 1105–1111.
[31] N. Chaari, J. Bischoff, K. Buchanan, C. Delafoy, P. Barberis, J. Augereau, K. Nimishakavi, The behavior of Cr-coated zirconium alloy cladding tubes at high temperatures, in: A. Motta, S. Yagnik (Eds.), Zirconium in the Nuclear Industry: 19th International Symposium, ASTM International, West Conshohocken, PA, 2021, pp. 189–210.
[32] E.J. Opila, Volatility of common protective oxides in high-temperature water vapor: current understanding and unanswered questions, Mater. Sci. Forum 461-464 (2004) 765–774.
[33] OECD-NEA, "QUENCH-ATF project," 2020. [Online]. Available: https://www.oecd-nea.org/jcms/pl_36597/quench-atf-project.
[34] IAEA, "Testing and simulation for advanced technology and accident tolerant fuels (ATF-TS)," [Online]. Available: https://nucleus.iaea.org/sites/connect/NFEpublic/Pages/ATF-TS.aspx.